



# A Partial Loss-of-Function Variant in *AKT2* Is Associated With Reduced Insulin-Mediated Glucose Uptake in Multiple Insulin-Sensitive Tissues: A Genotype-Based Callback Positron Emission Tomography Study

Aino Latva-Rasku,<sup>1</sup> Miikka-Juhani Honka,<sup>1</sup> Alena Stančáková,<sup>2</sup> Heikki A. Koistinen,<sup>3,4</sup> Johanna Kuusisto,<sup>2,5</sup> Li Guan,<sup>6</sup> Alisa K. Manning,<sup>7,8,9</sup> Heather Stringham,<sup>6</sup> Anna L. Gloyn,<sup>10,11,12</sup> Cecilia M. Lindgren,<sup>7,10,13</sup> T2D-GENES Consortium, Francis S. Collins,<sup>14</sup> Karen L. Mohlke,<sup>15</sup> Laura J. Scott,<sup>6</sup> Tomi Karjalainen,<sup>1</sup> Lauri Nummenmaa,<sup>1,16</sup> Michael Boehnke,<sup>6</sup> Pirjo Nuutila,<sup>1,17</sup> and Markku Laakso<sup>2,5</sup>

*Diabetes* 2018;67:334–342 | <https://doi.org/10.2337/db17-1142>

Rare fully penetrant mutations in *AKT2* are an established cause of monogenic disorders of glucose metabolism. Recently, a novel partial loss-of-function *AKT2* coding variant (p.Pro50Thr) was identified that is nearly specific to Finns (frequency 1.1%), with the low-frequency allele associated with an increase in fasting plasma insulin level and risk of type 2 diabetes. The effects of the p.Pro50Thr *AKT2* variant (p.P50T/*AKT2*) on insulin-stimulated glucose uptake (GU) in the whole body and in different tissues have not previously been investigated. We identified carriers ( $N = 20$ ) and matched noncarriers ( $N = 25$ ) for this allele in the population-based Metabolic Syndrome in Men (METSIM) study and invited these individuals back for positron emission tomography study with [<sup>18</sup>F]-fluorodeoxyglucose during euglycemic hyperinsulinemia. When we compared p.P50T/*AKT2* carriers to noncarriers, we found a 39.4% reduction in whole-body GU ( $P = 0.006$ ) and a 55.6%

increase in the rate of endogenous glucose production ( $P = 0.038$ ). We found significant reductions in GU in multiple tissues—skeletal muscle (36.4%), liver (16.1%), brown adipose (29.7%), and bone marrow (32.9%)—and increases of 16.8–19.1% in seven tested brain regions. These data demonstrate that the p.P50T substitution of *AKT2* influences insulin-mediated GU in multiple insulin-sensitive tissues and may explain, at least in part, the increased risk of type 2 diabetes in p.P50T/*AKT2* carriers.

Many large-scale exome and genome sequencing studies currently are under way to identify low-frequency and rare genetic variants associated with human diseases and traits. Large samples typically are required to obtain convincing association evidence for such variants. Once a rare-variant association is identified, investigators may call back carriers

<sup>1</sup>Turku PET Centre, University of Turku, Turku, Finland

<sup>2</sup>Internal Medicine, Institute of Clinical Medicine, University of Eastern Finland, Kuopio, Finland

<sup>3</sup>University of Helsinki and Department of Medicine, Helsinki University Central Hospital, Helsinki, Finland

<sup>4</sup>Minerva Foundation Institute for Medical Research, Helsinki, Finland

<sup>5</sup>Department of Medicine, Kuopio University Hospital, Kuopio, Finland

<sup>6</sup>Department of Biostatistics and Center for Statistical Genetics, University of Michigan, Ann Arbor, MI

<sup>7</sup>Program in Medical and Population Genetics, Broad Institute, Cambridge, MA

<sup>8</sup>Clinical and Translational Epidemiology Unit, Massachusetts General Hospital, Boston, MA

<sup>9</sup>Department of Medicine, Harvard Medical School, Boston, MA

<sup>10</sup>Wellcome Trust Centre for Human Genetics, Nuffield Department of Medicine, University of Oxford, Oxford, U.K.

<sup>11</sup>Oxford Centre for Diabetes, Endocrinology and Metabolism, Radcliffe Department of Medicine, University of Oxford, Oxford, U.K.

<sup>12</sup>National Institute for Health Research Oxford Biomedical Research Centre, Oxford University Hospitals NHS Foundation Trust, Oxford, U.K.

<sup>13</sup>Big Data Institute, Li Ka Shing Centre for Health Information and Discovery, University of Oxford, Oxford, U.K.

<sup>14</sup>National Human Genome Research Institute, National Institutes of Health, Bethesda, MD

<sup>15</sup>Department of Genetics, University of North Carolina at Chapel Hill, Chapel Hill, NC

<sup>16</sup>Department of Psychology, University of Turku, Finland

<sup>17</sup>Department of Endocrinology, Turku University Hospital, Turku, Finland

Corresponding authors: Markku Laakso, [markku.laakso@uef.fi](mailto:markku.laakso@uef.fi), Pirjo Nuutila, [pirjo.nuutila@utu.fi](mailto:pirjo.nuutila@utu.fi), and Michael Boehnke, [boehnke@umich.edu](mailto:boehnke@umich.edu).

Received 21 September 2017 and accepted 7 November 2017.

M.B., P.N., and M.L. shared last authorship.

© 2017 by the American Diabetes Association. Readers may use this article as long as the work is properly cited, the use is educational and not for profit, and the work is not altered. More information is available at <http://www.diabetesjournals.org/content/license>.

and noncarriers of the associated variant from the study population and undertake additional phenotyping to help understand disease mechanism. Such phenotyping might not have been considered at study outset or might have been too costly to undertake in the full study sample. Finland provides an ideal base for genotype callback studies. The history of Finland, with recent population bottlenecks, has resulted in increased frequency of genetic variants that are rare elsewhere, including nonsynonymous and particularly loss-of-function variants (1). Further, Finland boasts a well-educated population strongly supportive of biomedical research. In our present study we applied this callback approach to investigate the effects of a partial loss-of-function variant p.Pro50Thr (rs184042322) *AKT2* (V-AKT Murine Thymoma Viral Oncogene Homolog 2) (p.P50T/*AKT2*) on the rates of glucose uptake (GU) in whole body and in multiple insulin-sensitive tissues to understand the mechanisms explaining increased risk of type 2 diabetes in p.P50T/*AKT2* carriers.

The *AKT2* protein plays a key role in the conserved phosphoinositide 3-kinase signaling pathway, downstream of the insulin receptor, and mediates the physiological effects of insulin in several tissues including liver, skeletal muscle, and adipose tissue (2–4). Additionally, *AKT2* is expressed in the bone marrow, heart, brain, small intestine, and kidney. Mice deficient in *Akt2* develop hyperglycemia, hyperinsulinemia, insulin resistance, age-dependent loss of adipose tissue, and diabetes in males (1,5).

In humans, rare penetrant mutations in the *AKT2* gene encoding AKT serine/threonine kinase 2 have been previously associated with monogenic disorders of glucose metabolism. The first p.Arg274His mutation described in a single family showed autosomal dominant inheritance of severe insulin resistance and diabetes and disrupted insulin signaling in cultured cells. Individuals with this loss-of-function mutation were unable to phosphorylate glycogen synthase kinase 3 (GSK3) in an in vitro kinase assay (6). In contrast, another mutation, p.Glu17Lys, caused severe fasting hypoinsulinemic hypoglycemia. *AKT2* p.Glu17Lys was constitutively located at the plasma membrane (7) and overexpression induced translocation of glucose transporter type 4 (GLUT4) to the plasma membrane (8).

In a recent meta-analysis of exome genotype data on 33,231 individuals of European ancestry without diabetes, investigators demonstrated that carriers of the low-frequency amino acid substitution p.P50T/*AKT2* had on average a 12% (95% CI 7–18%,  $P = 1.0 \times 10^{-9}$ ) increase in fasting insulin level and an increased risk of type 2 diabetes (allele-specific odds ratio 1.05,  $P = 8.1 \times 10^{-5}$ ) (9). In vitro studies demonstrated the variant protein leads to a partial loss of *AKT2* phosphorylation at its activation sites (Thr308 and Ser473), suggesting impaired *AKT2* signaling and a reduced ability to phosphorylate its downstream target GSK3 $\beta$  (9). The p.P50T/*AKT2* variant was found at a frequency of 1.1% in Finns, but it was present at much lower frequencies in other ancestries (minor allele frequency 0.2% in non-Finnish Europeans and  $\leq 0.01\%$  in African American, Asian,

and Hispanic individuals), making Finland the ideal place for more detailed genotype-phenotype investigations.

## RESEARCH DESIGN AND METHODS

### The METSIM Positron Emission Tomography Studies

#### Study Participants

We selected male participants from the ongoing Metabolic Syndrome in Men (METSIM) follow-up study with ( $N = 20$ , 1 homozygous, 19 heterozygous) and without ( $N = 25$ ) p.P50T/*AKT2* and matched for age and BMI (10,11). They fulfilled the following inclusion criteria: age 50–75 years, BMI 20–40 kg/m<sup>2</sup>, and an oral glucose tolerance test not indicating diabetes. We applied the following exclusion criteria: diabetes, a chronic disease that could affect glucose metabolism (e.g., liver, kidney, thyroid, cancer), abusive use of alcohol, and any chronic medication that could affect glucose metabolism (e.g., steroids,  $\beta$ -blockers, thiazide diuretics, antipsychotics, antidepressants). We performed positron emission tomography (PET) studies at the PET Centre of the University of Turku, Finland. Assuming the sample sizes of 20 and 25 in the two groups, we had 80% power at significance level  $\alpha = 0.05$  to detect a 30% difference in the means of skeletal muscle GU based on previous studies performed at the Centre. The Ethics Committee of the Hospital District of Southwest Finland approved the study protocol. The study was conducted according to the principles of the Declaration of Helsinki. All participants gave written informed consent prior to participation in the study.

#### Genotyping

We originally genotyped the participants of the METSIM study on the Illumina HumanExome Beadchip (9). We confirmed the p.P50T/*AKT2* genotypes with TaqMan Allelic Discrimination Assays (Applied Biosystems) for PET study participants.

#### Hyperinsulinemic-Euglycemic Clamp

We performed a hyperinsulinemic-euglycemic clamp after an overnight fast of 10–12 h. Two catheters were inserted in veins of opposite forearms: one in the right antecubital vein for blood sampling and another in the left forearm for glucose and insulin infusions and radiotracer injection. To obtain arterialized venous plasma, the right arm was warmed. After catheterization, we collected baseline samples and performed the hyperinsulinemic-euglycemic clamp as previously described (12) with the insulin infusion rate of 40 mU/m<sup>2</sup> body surface area/min (Actrapid; Novo Nordisk, Copenhagen, Denmark). We maintained euglycemia by moderating the rate of 20% glucose infusion based on the plasma glucose level measured every 5–10 min. We reported the rates of whole-body GU (M value) as the average of 20-min intervals between 60–140 min after the start of insulin infusion.

#### GU Measurements Using PET/CT During the Hyperinsulinemic-Euglycemic Clamp

We quantified the rates of tissue-specific GU using the PET/CT (Discovery 690; GE Medical Systems, Milwaukee, WI), with 2-deoxy-2-[<sup>18</sup>F]fluoro-D-glucose (<sup>18</sup>F-FDG) as tracer.

The method of producing the tracer has been previously described (13). After reaching a steady euglycemia ( $69 \pm 15$  min from the start of insulin infusion), we injected participants with  $152 \pm 10$  MBq of  $^{18}\text{F}$ -FDG and started PET scanning. The scanned regions were heart (40 min), liver (15 min), upper abdomen (15 min), thigh skeletal muscle (15 min), neck (10 min), and brain (10 min). We performed all PET measurements blinded to AKT2 genotype.

### Endogenous Glucose Production

We collected a urine sample immediately after GU measurements and measured the amount of radiotracer lost into urine using an isotope dose calibrator (Model VDC-205; Comcer Netherlands, Joure, Netherlands). We assessed endogenous glucose production (EGP) by subtracting glucose infusion rate from rate of glucose disposal derived from  $^{18}\text{F}$ -FDG consumption (14). The liver produces  $\sim 80\%$  of EGP and the kidney  $\sim 20\%$  (15).

### Nonbrain PET GU

Before analysis, we corrected imaging data for dead time, decay, and photon attenuation. To determine the input function, we calculated a blood time-activity curve by combining arterial blood activity data from the PET images (first 10 min after injection) with measurements made from arterialized venous blood plasma samples collected at nine time points (5, 10, 20, 30, 40, 47.5, 62.5, 75, and 85 min after injection) during the scanning (16). We determined plasma activity using an automatic gamma counter (Wizard 1480 3; Wallac, Turku, Finland). We derived tissue activity and fractional uptake ( $K_i$ ) of the tracer from graphical analyses (17) applying the Carimas Software (version 2.9, Turku PET Centre, downloadable at <http://www.turkupetcentre.fi/software/>). We used a segmenting tool for myocardium to include the left ventricle wall and septum in the analysis; for other tissues the regions of interest (ROIs) were drawn manually. For skeletal muscle analysis, ROIs were drawn to include the medial parts of quadriceps femoris muscle of both thighs; for the liver, a section of the right lobe free of large vessels was chosen. The same researcher (A.L.-R.) performed analyses blinded and estimated the rates of skeletal muscle and liver GU twice for the first 24 participants. The Pearson correlation between the two measurements was 0.99 for skeletal muscle and 0.92 for liver.

We report the average of several ROIs for different adipose tissue types, with subcutaneous adipose tissue ROIs positioned around waistline, visceral adipose tissue ROIs in intraperitoneal cavity, and brown adipose tissue ROIs in supraclavicular areas on both sides of the neck. Bone marrow ROIs were drawn inside the body of both femoral bones and reported as their average.

### Brain PET GU

We carried out preprocessing and statistical analyses of the brain PET images with the SPM 12 software (<http://www.fil.ion.ucl.ac.uk/spm/>). We first normalized PET images into an in-house  $^{18}\text{F}$ -FDG template according to the Montreal Neurological Institute standard using linear and nonlinear

transformations and smoothed with a Gaussian kernel with 8-mm full width at half maximum. Next, we quantified the voxelwise fractional uptake rate as the ratio of tissue time activity and integral of plasma activity from time 0 to the time of the scan. We compared voxelwise between-group differences in fractional uptake rate using a nonparametric full-volume analysis in the SnPM13 toolbox (<http://warwick.ac.uk/snpm>). We constructed anatomical ROIs in the brain lobes, midbrain, limbic system, and cerebellum in a manner parallel to that for the other tissues.

### Calculation of Tissue-Specific GU

To assess the rates of tissue-specific GU ( $\mu\text{mol/kg/min}$ ), we multiplied tissue fractional uptake by plasma glucose concentration during scanning and divided by tissue density and a previously established lumped constant: 1.2 for skeletal muscle, 1.0 for myocardium and liver, 1.14 for adipose tissue, 1.1 for intestine, and 0.65 for brain (18–24). The lumped constant for bone marrow has not been defined, so we adopted the previously used value of 1.0 (25) to compare the results between groups.

### Laboratory Measurements

We measured plasma glucose in duplicates using the glucose oxidase method (Analog GM9; Analog Instruments, London, UK) in the fasting state and during the clamp. We determined plasma insulin levels in the fasting state and at 30-min intervals after the start of insulin infusion until the end of clamp using an automated electrochemiluminescence immunoassay (Cobas 8000; Roche Diagnostics, Mannheim, Germany). We measured serum free fatty acid (FFA) levels in the fasting state and at 60-min intervals during the clamp with an enzymatic colorimetric method assay (NEFA-HR2, ACS-ACOD; Wako Chemicals, Neuss, Germany; Cobas 8000 c502 Analyzer, Roche Diagnostics).

### Statistical Analyses

We carried out data analyses with IBM SPSS 21.0 for Windows (Chicago, IL). We give the results for continuous variables as means  $\pm$  SD. We logarithm transformed variables with skewed distribution (insulin, triacylglycerol, FFA, GU in subcutaneous and visceral adipose tissue) prior to statistical analyses. We assessed the differences between the groups by the independent samples *t* test for continuous variables and  $\chi^2$  test for discrete variables. We used linear regression to adjust the results for outside temperature in the previous 30, 14, and 7 days in statistical analyses of brown adipose tissue GU. We assessed the correlation between different measures of GU by the Spearman correlation coefficient. We used the Fisher *r*-to-*z* transformation to compare correlation coefficients in carriers and noncarriers of the p.P50T/AKT2. The threshold for statistical significance was set at  $\alpha = 0.05$ .

## RESULTS

### The Euglycemic-Hyperinsulinemic Clamp and PET Study

#### Characteristics of the Participants

Characteristics of the p.P50T/AKT2 carriers ( $N = 20$ , 1 homozygous, 19 heterozygous) and noncarriers ( $N = 25$ ) without

chronic diseases are presented in Table 1. These two groups of participants were matched for age and BMI and did not differ significantly by age, BMI, or fasting glucose. As expected, fasting insulin was higher in the p.P50T/AKT2 carriers than in the noncarriers. We pooled the single p.P50T/AKT2 homozygous carrier with heterozygous carriers in all statistical analysis because the homozygous carrier was not an outlier among the group of carriers.

### Whole-Body GU, Glucose Disposal, and EGP

Whole-body GU was assessed by the euglycemic-hyperinsulinemic clamp-based M value and the glucose disposal rate by the  $^{18}\text{F}$ -FDG disappearance rate (20). To verify the quality of the euglycemic-hyperinsulinemic clamp, we compared the mean glucose levels during the clamp in p.P50T/AKT2 carriers and noncarriers; we observed essentially no difference between the two groups ( $5.0 \pm 0.4$  and  $5.0 \pm 0.2$  mmol/L,  $P = 0.53$ ). The rates of whole-body GU ( $17.6 \pm 10.3$  vs.  $29.2 \pm 15.2$   $\mu\text{mol/kg/min}$ ,  $P = 0.006$ ) and glucose disposal ( $25.6 \pm 9.9$  vs.  $33.1 \pm 11.9$   $\mu\text{mol/kg/min}$ ,  $P = 0.029$ ) were lower in p.P50T/AKT2 carriers compared with noncarriers (Fig. 1A). EGP during the clamp was higher in p.P50T/AKT2 carriers than in noncarriers ( $9.0 \pm 2.6$  vs.  $5.8 \pm 6.9$   $\mu\text{mol/kg/min}$ ,  $P = 0.038$ ).

### Tissue-Specific GU

We assessed GU in different tissues using the euglycemic-hyperinsulinemic clamp and PET. We observed lower rates of GU in carriers of the p.P50T/AKT2 variant compared with noncarriers in skeletal muscle ( $23.9 \pm 14.1$  vs.  $37.5 \pm 20.7$   $\mu\text{mol/kg/min}$ ,  $P = 0.012$ ), liver ( $21.0 \pm 5.1$  vs.  $25.1 \pm 6.6$   $\mu\text{mol/kg/min}$ ,  $P = 0.030$ ), brown adipose tissue ( $11.7 \pm 5.1$  vs.  $16.7 \pm 6.9$   $\mu\text{mol/kg/min}$ ,  $P = 0.004$ ), and bone marrow ( $13.3 \pm 5.4$  vs.  $19.8 \pm 8.8$   $\mu\text{mol/kg/min}$ ,

$P = 0.004$ ) (Fig. 1B and C), but did not observe significant differences in subcutaneous adipose tissue ( $11.3 \pm 4.1$  vs.  $12.7 \pm 5.8$   $\mu\text{mol/kg/min}$ ,  $P = 0.488$ ), visceral adipose tissue ( $17.3 \pm 6.4$  vs.  $20.9 \pm 8.5$   $\mu\text{mol/kg/min}$ ,  $P = 0.157$ ), myocardium ( $34.2 \pm 16.8$  vs.  $35.0 \pm 12.6$   $\mu\text{mol/100 g/min}$ ,  $P = 0.870$ ), duodenum ( $31.9 \pm 7.0$  vs.  $31.7 \pm 7.1$   $\mu\text{mol/kg/min}$ ,  $P = 0.931$ ), or jejunum ( $33.2 \pm 7.0$  vs.  $32.4 \pm 7.2$   $\mu\text{mol/kg/min}$ ,  $P = 0.711$ ). We observed higher rates of GU in the p.P50T/AKT2 carriers than in noncarriers in all seven analyzed brain regions ( $P = 0.001$ ) (Fig. 2).

### FFA Levels in Fasting and During the Clamp

Fasting FFA levels did not differ between carriers and noncarriers of p.P50T/AKT2 ( $0.43 \pm 0.16$  vs.  $0.39 \pm 0.16$  mmol/L,  $P = 0.360$ ). However, FFA levels were higher during hyperinsulinemia at 60 min in carriers than in noncarriers of p.P50T/AKT2 ( $0.16 \pm 0.12$  vs.  $0.09 \pm 0.05$  mmol/L,  $P = 0.024$ ).

### Correlations Between the Rates of Whole-Body and Brain GU With Tissue-Specific GU and EGP in Carriers and Noncarriers of p.P50T/AKT2

The differences in the rates of GU across several tissues between carriers and noncarriers of p.P50T/AKT2 we observed prompted us to investigate the correlations of the rates of GU separately in carriers and noncarriers of p.P50T/AKT2. Whole-body GU correlated positively with skeletal muscle GU ( $r = 0.92$  vs.  $r = 0.90$ ), bone marrow GU ( $r = 0.74$  vs.  $r = 0.85$ ), subcutaneous fat GU ( $r = 0.59$  vs.  $r = 0.40$ ), and liver GU ( $r = 0.41$  vs.  $r = 0.46$ ), and negatively with brain GU ( $r = -0.56$  vs.  $r = -0.66$ ) in both noncarriers and carriers of p.P50T/AKT2, respectively (Fig. 3A). Correlations of the rates of whole-body GU with brown fat GU ( $r = 0.80$  vs.  $r = 0.36$ ,  $P = 0.023$ ) and EGP in the liver ( $r = -0.41$  vs.  $-0.08$ ,  $P = 0.276$ ) were substantially weaker

**Table 1—Clinical and laboratory characteristics of the p.P50T/AKT2 noncarriers and carriers who participated in the METSIM PET studies**

Variable	Noncarriers (N = 25)	Carriers (N = 20)	P value
Age, years	63.9 $\pm$ 4.8	61.9 $\pm$ 6.3	0.23
Height, cm	176.9 $\pm$ 5.3	174.2 $\pm$ 5.5	0.10
Weight, kg	87.4 $\pm$ 10.2	86.1 $\pm$ 11.6.2	0.70
BMI, kg/m <sup>2</sup>	28.1 $\pm$ 3.4	28.7 $\pm$ 3.4	0.60
Waist, cm	100.7 $\pm$ 8.9	100.3 $\pm$ 8.7	0.88
Fat mass, %	29.0 $\pm$ 7.0	28.0 $\pm$ 7.0	0.60
Systolic blood pressure, mmHg	133.8 $\pm$ 14.1	137.3 $\pm$ 15.9	0.44
Diastolic blood pressure, mmHg	86.4 $\pm$ 10.1	86.6 $\pm$ 8.5	0.94
Fasting plasma glucose, mmol/L	6.0 $\pm$ 6.5	6.1 $\pm$ 0.3	0.28
Fasting insulin, mU/L	9.4 $\pm$ 5.6	17.8 $\pm$ 10.2	0.003
LDL cholesterol, mmol/L	3.30 $\pm$ 0.96	2.92 $\pm$ 1.09	0.21
HDL cholesterol, mmol/L	1.51 $\pm$ 0.38	1.33 $\pm$ 0.37	0.12
Total triglycerides, mmol/L	1.12 $\pm$ 0.50	1.48 $\pm$ 1.04	0.26
Alanine transferase, units/L	29.7 $\pm$ 13.6	32.6 $\pm$ 17.8	0.58
Creatinine, $\mu\text{mol/L}$	85.3 $\pm$ 10.5	85.5 $\pm$ 12.6	0.96

Data are mean  $\pm$  SD. Total triglycerides and alanine transferase were log-transformed to calculate P value.

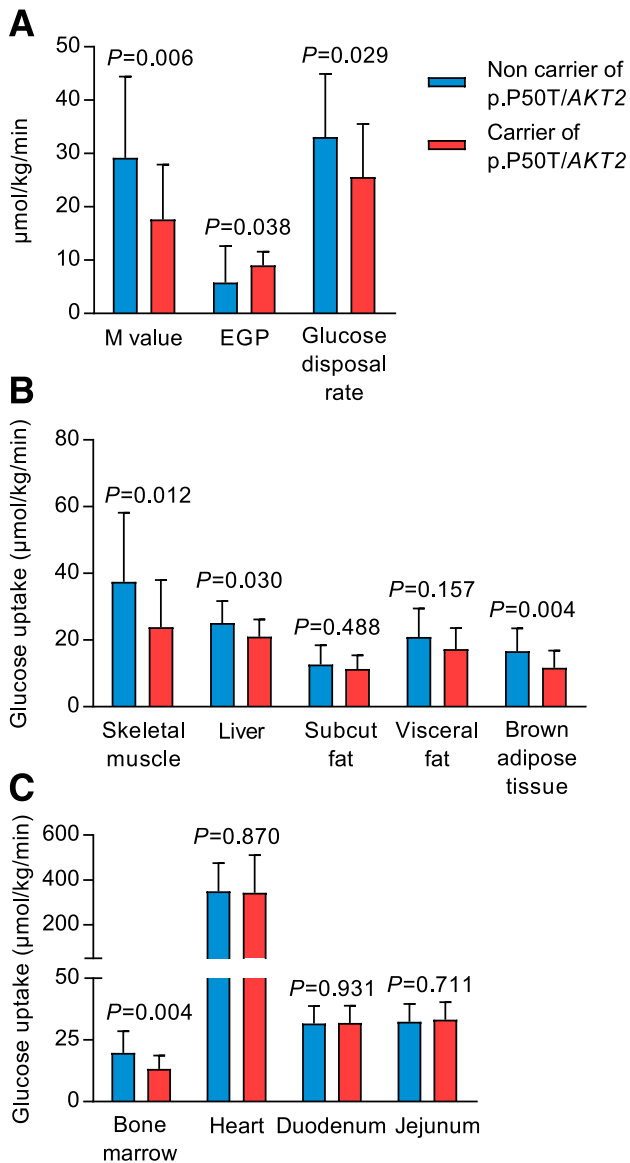


**Figure 1**—Whole-body and tissue-specific GU. **A:** Whole-body GU (M value), EGP, and whole-body glucose disposal rate in the carriers (red bars,  $N = 20$ ) and noncarriers (blue bars,  $N = 25$ ) of p.P50T/AKT2. **B** and **C:** Tissue-specific GU in the carriers (red bars,  $N = 20$ ) and noncarriers (blue bars,  $N = 25$ ) of p.P50T/AKT2. Bar heights represent sample means, vertical lines represent sample SDs.  $P$  values for comparison of carriers versus noncarriers of p.P50T/AKT2. Subcut, subcutaneous.

among the carriers than among noncarriers of p.P50T/AKT2. Whole-body GU correlated weakly with heart muscle GU and jejunum GU without any substantial difference between the noncarriers and carriers of p.P50T/AKT2. Correlations of brain GU with EGP ( $r = 0.68$  vs.  $r = 0.05$ ,  $P = 0.016$ ) and bone marrow GU ( $r = -0.24$  vs.  $r = -0.84$ ,  $P = 0.002$ ) were significantly different between the noncarriers and carriers of p.P50T/AKT2 (Fig. 3B).

## DISCUSSION

Our genotype-based callback PET study demonstrates that a low-frequency partial loss-of-function p.P50T/AKT2 variant,

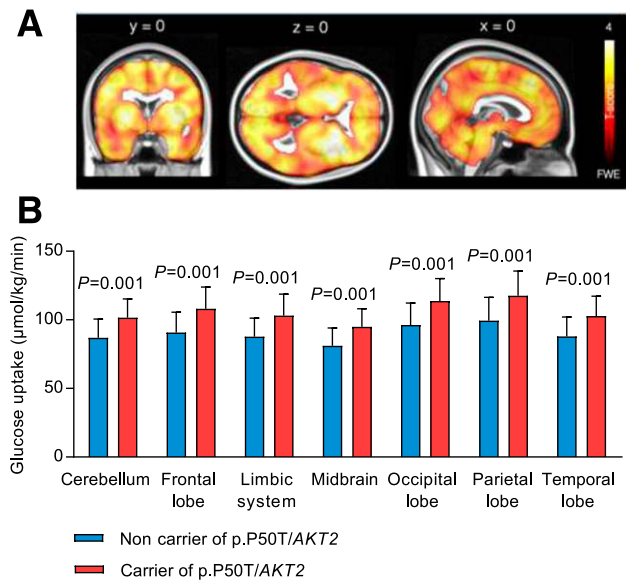


**Figure 2**—**A:** Brain regions in the PET study where insulin-stimulated GU was measured in carriers and noncarriers of the p.P50T/AKT2 variant. **B:** Significant differences ( $P$  value) in GU in the specific regions of the brain between noncarriers (blue bars,  $N = 25$ ) and carriers (red bars,  $N = 20$ ) of the p.P50T/AKT2 variant. Data are mean  $\pm$  SD.

nearly unique to Finns and probably originating from a recent bottleneck in the 16th century in the settlement of Eastern Finland (1), is associated with significantly decreased GU in whole body and in multiple insulin-sensitive tissues. This is consistent with our previous study (9) demonstrating that insulin levels were increased in carriers of p.P50T/AKT2 as a compensatory mechanism for insulin resistance. The increase in insulin levels was substantially less in carriers of p.P50T/AKT2 compared with carriers of the p.Arg274His/AKT2 loss-of-function mutation previously reported (6).

Activation of AKT2 is associated with translocation of GLUT4 from intracellular storage vesicles to the cell surface (26,27). AKT2 is the major isoform of AKT and is abundantly expressed in skeletal muscle (8,9). Insulin-stimulated AKT2 activation leads to inactivation of GSK3 $\beta$  (3,28), resulting in increased glycogen synthesis. Moreover, gene silencing experiments have provided evidence that AKT2 is indispensable for insulin action on glucose uptake and glycogen synthesis in human skeletal muscle cells (29). The current study shows that in vivo skeletal muscle GU was reduced by 36% ( $P = 0.012$ ) in the p.P50T/AKT2 carriers compared with noncarriers. This could be explained, at least in part, by reduced activity of the low-frequency p.P50T/AKT2 variant, in agreement with our previous finding of impaired insulin signaling in HeLa cells and human liver HuH7 cells for the variant (9). Collectively, these findings demonstrate that AKT2 is an important determinant of insulin sensitivity in human skeletal muscle.

The liver plays an important role in maintaining normal glucose levels by regulating EGP (gluconeogenesis) and glycogenolysis (glycogen breakdown). Additionally, the kidney



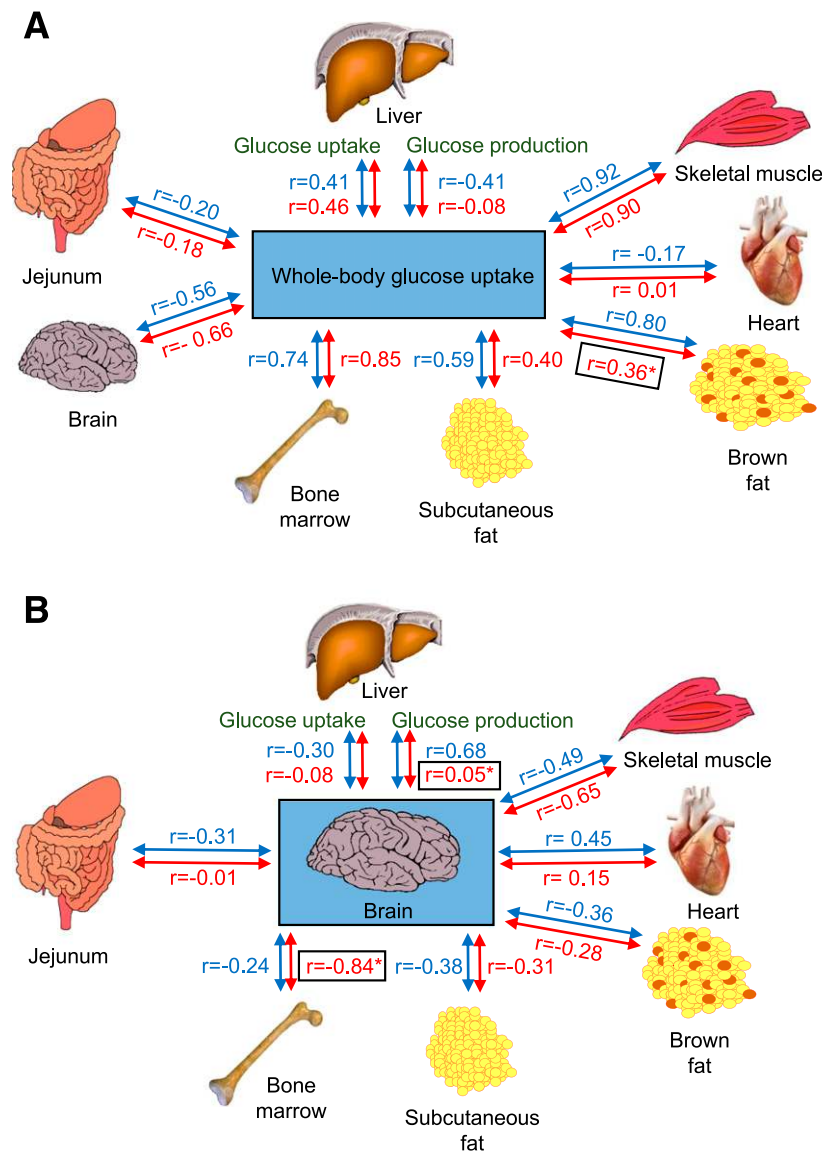


**Figure 3**—A: Correlations of whole-body GU with the tissue-specific GU in skeletal muscle, heart muscle, brown fat, subcutaneous fat, bone marrow, brain, jejunum, and liver in carriers and noncarriers of the p.P50T/AKT2 variant. B: Correlations of the mean brain GU with tissue-specific GU in skeletal muscle, heart muscle, brown fat, subcutaneous fat, bone marrow, jejunum, and liver in carriers and noncarriers of the p.P50T/AKT2 variant. Blue indicates correlations in noncarriers and red in carriers of the p.P50T/AKT2 variant. \**P* < 0.05 (exact *P* values are given in the text) for correlations that were significantly different between carriers and noncarriers of the p.P50T/AKT2 variant.

produces about 20% of EGP (15). Normally, insulin suppresses EGP and inhibits the genes encoding gluconeogenesis and redirects newly synthesized glucose-6-phosphate to glycogen (3). We found that EGP was significantly increased and liver GU decreased in the carriers of the AKT2 variant compared with noncarriers, indicating liver insulin resistance. AKT2 plays an important role in the regulation of liver and kidney (29) insulin sensitivity. AKT2 phosphorylates and inhibits FOXO1, a key regulator of EGP (30). Our findings agree with the results observed in mice deficient in Akt2, which demonstrated a significant failure of insulin to suppress EGP (2). Additionally, we found that liver GU was decreased in the carriers of the p.P50T/AKT2 variant compared with noncarriers. This could be due to impaired

insulin signaling attributable to the p.P50T/AKT2 variant, which results in subnormal inactivation of GSK3β. Other mechanisms, independent of GSK3β suppression, could also play a role, as recently suggested (3).

Activation of AKT2 enhances GLUT4 translocation and the rates of GU similarly in adipose tissue and skeletal muscle (6). GU into the white adipose tissue is relatively minor, accounting for only 5–10% of whole-body GU during insulin-stimulated states, suggesting that white adipose tissue does not have a major quantitative role in postprandial glucose metabolism (31,32). We did not find a statistically significant difference between the carriers and noncarriers of p.P50T/AKT2 in the rates of GU in subcutaneous or visceral adipose tissue, although the rates of GU were slightly



genotype-based callback studies and the practicality of PET as an informative, noninvasive method to characterize the function of genetic variants of interest.

**Acknowledgments.** The authors thank the 45 volunteers who participated in this study.

**Funding.** The authors acknowledge the following funding sources: National Institutes of Health National Heart, Lung, and Blood Institute (NIH/NHLBI 5K01DK107836) (A.K.M.); the Wellcome Trust (095101/Z/10/Z and 200837/Z/16/Z) (A.L.G.); Medical Research Council (MR/L020149/1) (A.L.G.); the Li Ka Shing Foundation (C.M.L.); the National Institute for Health Research Oxford Biomedical Research Centre (C.M.L.); Widenlife (C.M.L.); National Institutes of Health grants CRR00070 CR00.01 (C.M.L.), R01DK093757 (K.L.M.), R01DK072193 (K.L.M.), and U01DK062370 (M.B.); and National Human Genome Research Institute Division of Intramural Research project number Z01HG000024 (F.S.C.). Sequence data were generated by the T2D-GENES Consortium with support from National Institutes of Health National Institute of Diabetes and Digestive and Kidney Diseases grants U01DK085501, U01DK085524, U01DK085526, U01DK085545, and U01DK085584; Suomen Akatemia (Academy of Finland) (321428) (M.L.); Juselius Foundation (M.L.); Sydäntutkimussäätiö (Finnish Foundation for Cardiovascular Research) (M.L.); European Medical Information Framework grant IMI JU GA 115372-2 (M.L.); Kuopion Yliopistollinen Sairaala (Kuopio University Hospital) VTR grant (M.L.); and Centre of Excellence of Cardiovascular and Metabolic Diseases supported by the Academy of Finland (P.N., M.L.). A.L.G. is a Wellcome Trust Senior Fellow in Basic Biomedical Research.

**Duality of Interest.** No potential conflicts of interest relevant to this article were reported.

**Author Contributions.** A.L.-R., M.-J.H., A.S., H.A.K., J.K., T.K., L.N., P.N., and M.L. contributed to sample collection and phenotyping. A.K.M., H.S., A.L.G., C.M.L., F.S.C., K.L.M., L.J.S., and M.B. contributed to data production (genotyping). A.L.-R., A.S., L.G., L.J.S., T.K., L.N., M.B., and M.L. contributed to statistical analysis. A.L.-R., M.-J.H., A.S., P.N., and M.L. contributed to study design. L.N., M.B., P.N., and M.L. contributed to study supervision. M.L. is the guarantor of this work and, as such, had full access to all the data in the study and takes responsibility for the integrity of the data and the accuracy of the data analysis.

**Prior Presentation.** The results were previously presented at the 77th Scientific Sessions of the American Diabetes Association, San Diego, CA, 9–13 June 2017, with the title “A Partial Loss of Function Variant in the AKT2 Gene Is Associated With Reduced Insulin-Mediated Glucose Uptake in Skeletal Muscle, Liver, Brown Adipose Tissue, and Bone Marrow: A Positron Emission Tomography Study” (18-OR).

## References

- Lim ET, Würtz P, Havulinna AS, et al.; Sequencing Initiative Suomi (SISU) Project. Distribution and medical impact of loss-of-function variants in the Finnish founder population. *PLoS Genet* 2014;10:e1004494
- Cho H, Mu J, Kim JK, et al. Insulin resistance and a diabetes mellitus-like syndrome in mice lacking the protein kinase Akt2 (PKB beta). *Science* 2001;292:1728–1731
- Wan M, Leavens KF, Hunter RW, et al. A noncanonical, GSK3-independent pathway controls postprandial hepatic glycogen deposition. *Cell Metab* 2013;18:99–105
- Koren S, DiPilato LM, Emmett MJ, et al. The role of mouse Akt2 in insulin-dependent suppression of adipocyte lipolysis in vivo. *Diabetologia* 2015;58:1063–1070
- Garofalo RS, Orena SJ, Rafidi K, et al. Severe diabetes, age-dependent loss of adipose tissue, and mild growth deficiency in mice lacking Akt2/PKB beta. *J Clin Invest* 2003;112:197–208
- George S, Rochford JJ, Wolfrum C, et al. A family with severe insulin resistance and diabetes due to a mutation in *AKT2*. *Science* 2004;304:1325–1328
- Hussain K, Challis B, Rocha N, et al. An activating mutation of *AKT2* and human hypoglycemia. *Science* 2011;334:474
- Gonzalez I, Tripathi G, Carter EJ, et al. Akt2, a novel functional link between p38 mitogen-activated protein kinase and phosphatidylinositol 3-kinase pathways in myogenesis. *Mol Cell Biol* 2004;24:3607–3622
- Manning A, Highland HM, Gasser J, et al. A low-frequency inactivating *AKT2* variant enriched in the Finnish population is associated with fasting insulin levels and type 2 diabetes risk. *Diabetes* 2017;66:2019–2032
- Stancáková A, Javorský M, Kuulasmaa T, Haffner SM, Kuusisto J, Laakso M. Changes in insulin sensitivity and insulin release in relation to glycemia and glucose tolerance in 6,414 Finnish men. *Diabetes* 2009;58:1212–1221
- Laakso M, Kuusisto J, Stancáková A, et al. The Metabolic Syndrome in Men study: a resource for studies of metabolic and cardiovascular diseases. *J Lipid Res* 2017;58:481–493
- DeFronzo RA, Tobin JD, Andres R. Glucose clamp technique: a method for quantifying insulin secretion and resistance. *Am J Physiol* 1979;237:E214–E223
- Harnacher K, Coenen HH, Stöcklin G. Efficient stereospecific synthesis of no-carrier-added 2-<sup>18</sup>F-fluoro-2-deoxy-D-glucose using aminopolyether supported nucleophilic substitution. *J Nucl Med* 1986;27:235–238
- Izzo P, Gastaldelli A, Järvisalo MJ, et al. <sup>18</sup>F-FDG assessment of glucose disposal and production rates during fasting and insulin stimulation: a validation study. *J Nucl Med* 2006;47:1016–1022
- Stumvoll M, Meyer C, Mitrakou A, Nadkarni V, Gerich JE. Renal glucose production and utilization: new aspects in humans. *Diabetologia* 1997;40:749–757
- Gambhir SS, Schwaiger M, Huang SC, et al. Simple noninvasive quantification method for measuring myocardial glucose utilization in humans employing positron emission tomography and fluorine-18 deoxyglucose. *J Nucl Med* 1989;30:359–366
- Patlak CS, Blasberg RG. Graphical evaluation of blood-to-brain transfer constants from multiple-time uptake data. Generalizations. *J Cereb Blood Flow Metab* 1985;5:584–590
- Peltoniemi P, Lönnroth P, Laine H, et al. Lumped constant for [(18)F]fluorodeoxyglucose in skeletal muscles of obese and nonobese humans. *Am J Physiol Endocrinol Metab* 2000;279:E1122–E1130
- Böttcher HE, Böttcher M, Schmitz O, et al. Glucose uptake and lumped constant variability in normal human hearts determined with [<sup>18</sup>F]fluorodeoxyglucose. *J Nucl Cardiol* 1997;4:125–132
- Izzo P, Järvisalo MJ, Kiss J, et al. Quantification of liver glucose metabolism by positron emission tomography: validation study in pigs. *Gastroenterology* 2007;132:531–542
- Virtanen KA, Peltoniemi P, Marjamäki P, et al. Human adipose tissue glucose uptake determined using [(18)F]-fluoro-deoxy-glucose ([<sup>18</sup>F]FDG) and PET in combination with microdialysis. *Diabetologia* 2001;44:2171–2179
- Orava J, Nuutila P, Lidell ME, et al. Different metabolic responses of human brown adipose tissue to activation by cold and insulin. *Cell Metab* 2011;14:272–279
- Honka H, Mäkinen J, Hannukainen JC, et al. Validation of [<sup>18</sup>F]fluorodeoxyglucose and positron emission tomography (PET) for the measurement of intestinal metabolism in pigs, and evidence of intestinal insulin resistance in patients with morbid obesity. *Diabetologia* 2013;56:893–900
- Wu HM, Bergsneider M, Glenn TC, et al. Measurement of the global lumped constant for 2-deoxy-2-<sup>18</sup>F-fluoro-D-glucose in normal human brain using [<sup>15</sup>O]-water and 2-deoxy-2-<sup>18</sup>F-fluoro-D-glucose positron emission tomography imaging. A method with validation based on multiple methodologies. *Mol Imaging Biol* 2003;5:32–41
- Huovinen V, Saunavaara V, Kiviranta R, et al. Vertebral bone marrow glucose uptake is inversely associated with bone marrow fat in diabetic and healthy pigs: [(18)F]FDG-PET and MRI study. *Bone* 2014;61:33–38
- Nozaki S, Takeda T, Kitauro T, Takenaka N, Kataoka T, Satoh T. Akt2 regulates Rac1 activity in the insulin-dependent signaling pathway leading to GLUT4 translocation to the plasma membrane in skeletal muscle cells. *Cell Signal* 2013;25:1361–1371
- Calera MR, Martinez C, Liu H, Jack AK, Birnbaum MJ, Pilch PF. Insulin increases the association of Akt-2 with Glut4-containing vesicles. *J Biol Chem* 1998;273:7201–7204



28. Cross DA, Alessi DR, Cohen P, Andjelkovich M, Hemmings BA. Inhibition of glycogen synthase kinase-3 by insulin mediated by protein kinase B. *Nature* 1995; 378:785–789
29. Bouzakri K, Zachrisson A, Al-Khalili L, et al. siRNA-based gene silencing reveals specialized roles of IRS-1/Akt2 and IRS-2/Akt1 in glucose and lipid metabolism in human skeletal muscle. *Cell Metab* 2006;4:89–96
30. Sasaki M, Sasako T, Kubota N, et al. Dual regulation of gluconeogenesis by insulin and glucose in the proximal tubules of the kidney. *Diabetes* 2017;66: 2339–2350
31. Sharabi K, Tavares CD, Rines AK, Puigserver P. Molecular pathophysiology of hepatic glucose production. *Mol Aspects Med* 2015;46:21–33
32. Virtanen KA, Lönnroth P, Parkkola R, et al. Glucose uptake and perfusion in subcutaneous and visceral adipose tissue during insulin stimulation in nonobese and obese humans. *J Clin Endocrinol Metab* 2002;87:3902–3910
33. Berggreen C, Gormand A, Omar B, Degerman E, Göransson O. Protein kinase B activity is required for the effects of insulin on lipid metabolism in adipocytes. *Am J Physiol Endocrinol Metab* 2009;296:E635–E646
34. Virtanen KA, Lidell ME, Orava J, et al. Functional brown adipose tissue in healthy adults. *N Engl J Med* 2009;360:1518–1525
35. Shearin AL, Monks BR, Seale P, Birnbaum MJ. Lack of AKT in adipocytes causes severe lipodystrophy. *Mol Metab* 2016;5:472–479
36. Krings A, Rahman S, Huang S, Lu Y, Czernik PJ, Lecka-Czernik B. Bone marrow fat has brown adipose tissue characteristics, which are attenuated with aging and diabetes. *Bone* 2012;50:546–552
37. Huovinen V, Bucci M, Lipponen H, et al. Femoral bone marrow insulin sensitivity is increased by resistance training in elderly female offspring of overweight and obese mothers. *PLoS One* 2016;11:e0163723
38. Kullmann S, Heni M, Hallschmid M, Fritsche A, Preissl H, Häring HU. Brain insulin resistance at the crossroads of metabolic and cognitive disorders in humans. *Physiol Rev* 2016;96:1169–1209
39. Hirvonen J, Virtanen KA, Nummenmaa L, et al. Effects of insulin on brain glucose metabolism in impaired glucose tolerance. *Diabetes* 2011;60:443–447
40. Tuulari JJ, Karlsson HK, Hirvonen J, et al. Weight loss after bariatric surgery reverses insulin-induced increases in brain glucose metabolism of the morbidly obese [published correction appears in *Diabetes* 2017;66:2724]. *Diabetes* 2013;62: 2747–2751
41. Zimmer ER, Parent MJ, Souza DG, et al. [<sup>18</sup>F]FDG PET signal is driven by astroglial glutamate transport. *Nat Neurosci* 2017;20:393–395
42. Heni M, Hennige AM, Peter A, et al. Insulin promotes glycogen storage and cell proliferation in primary human astrocytes. *PLoS One* 2011;6:e21594
43. Obici S, Zhang BB, Karkanas G, Rossetti L. Hypothalamic insulin signaling is required for inhibition of glucose production. *Nat Med* 2002;8:1376–1382